

Pultrusion of a vertical axis wind turbine blade part-II: combining the manufacturing process simulation with a subsequent loading scenario

Ismet Baran · Jesper H. Hattel · Cem C. Tutum · Remko Akkerman

Received: 22 December 2013 / Accepted: 11 May 2014 / Published online: 23 May 2014
© Springer-Verlag France 2014

Abstract This paper in particular deals with the integrated modeling of a pultruded NACA0018 blade profile being a part of EU funded *DeepWind* project. The manufacturing aspects of the pultrusion process are associated with the preliminary subsequent service loading scenario. A 3D thermo-chemical analysis of the pultrusion process is sequentially coupled with a 2D quasi-static mechanical analysis in which the process induced residual stresses and distortions are predicted using the generalized plane stain elements in a commercial finite element software ABAQUS. The temperature- and cure-dependent resin modulus is implemented by employing the cure hardening instantaneous linear elastic (CHILE) model in the process simulation. The subsequent bent-in place simulation of the pultruded blade profile is performed taking the residual stresses into account. The integrated numerical simulation tool predicts the internal stress levels of the profile at the end of the bending analysis. It is found that the process induced residual

stresses have the potential to influence the internal stresses arise in the structural analysis.

Keywords Pultrusion process · Residual/internal stress · Finite element analysis · Integrated modelling · Thermosetting resin.

Introduction

Pultrusion is a continuous manufacturing process in which constant cross sectional composite profiles are produced. A schematic view of the process is depicted in Fig. 1. The reinforcements (roving, continuous filament mat, etc.) are pulled through the pre-formers and wetted out in a thermosetting resin bath. The part is cured inside the heating die and cut into desired lengths by a cutting mechanism at the end of the process.

Pultruded products are foreseen to have potential for the replacement of some of the structural profiles such as the VAWT blades/components and the steel reinforcement of the concrete. The process has to be well characterized to improve the product quality in terms of the internal stress level arising during the service loading. The process induced residual stresses are generated by various mechanisms that inherently exist in the composite manufacturing processes such as the chemical shrinkage of the thermosetting resin and the mismatch in the coefficient of thermal expansion (CTE) of the reinforcement and the resin [1–3]. Therefore, the evolution of the process induced stresses as well as the distortions must be well investigated in order to have a better understanding of the mechanical behaviour of the pultruded products under service loading conditions. Since running a production line by trial and error is an expensive and time consuming task, the development of a numerical simulation

I. Baran (✉) · J. H. Hattel
Department of Mechanical Engineering, Technical
University of Denmark, 2800 Kgs. Lyngby, Denmark
e-mail: isbar@mek.dtu.dk

C. C. Tutum
Department of Electrical and Computer Engineering,
Michigan State University, East Lansing, MI, USA

R. Akkerman
Faculty of Engineering Technology, University of Twente,
NL-7500AE Enschede, The Netherlands

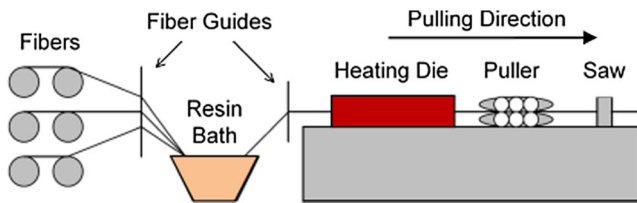


Fig. 1 Schematic view of a pultrusion process

tool to predict the process induced stresses and distortions is highly required. Using this tool, it can also be possible to take the manufacturing effects such as the residual stresses into account for the service loading simulations.

Pultrusion technology was used to manufacture a vertical axis wind turbine (VAWT) blade as reported in [4]. The pultruded blade was then shaped into a troposkien (*Darrieus* design). Similarly, pultrusion is currently being considered in EU funded *DeepWind* Project [5, 6] in which a novel design concept is developed for a floating offshore (VAWT) based on the *Darrieus* design.

In literature, the pultrusion process has been investigated both numerically and experimentally. The main aim has been to understand the process by evaluating the development of the resin flow [7–9], temperature [10–12] and degree of cure profiles [13–15]. In addition, the frictional

force inside the heating die has also been analysed in [16–18]. In these studies [7–18], well known numerical methods such as the finite difference method (FDM), the finite volume method (FVM) or the finite element method (FEM) have been utilized. All these contributions have only been dealing mainly with thermal modelling thus being able to predict characteristic temperature and cure degree behaviours for pultrusion. Typically the temperature of the composite is initially lagging behind the die temperature and subsequently it exceeds the die temperature during curing due to the internal heat generation of the resin [13]. In addition to these studies in the literature, the authors have contributed substantially with state-of-the-art models for pultrusion. This includes efficient thermo-chemical models [19, 20] together with performing probabilistic analysis of the process [21] and optimization simulations [22, 23]. Moreover, the authors have proposed the first models for the thermo-mechanical aspects of the pultrusion process including the evolution of the process induced stresses, distortions and mechanical properties [24, 25]. In these works [24, 25], a three dimensional (3D) transient thermo-chemical model is sequentially coupled with a 2D quasi static plane strain mechanical model for the pultrusion process using the FEM. This proposed approach, which is found to be computationally efficient, provides an increased understanding of the process by evaluating the development of the stresses and distortions as well as the mechanical properties during processing.

So far, an integrated modelling of a pultruded product particularly combining the manufacturing simulation with the subsequent service loading scenario has not been described in literature. The manufacturing aspects of the pultrusion process are hence associated with the subsequent loading simulation for the pultruded NACA0018 blade profile in the present work. More specifically, the residual stresses together with the final mechanical properties of the transversely isotropic pultruded product are subsequently transferred to the loading analysis in which a non-linear bending simulation of the NACA0018 profile is performed. A unidirectional (UD) glass/epoxy composite is considered for the process simulation. The temperature and the degree of cure profiles are first calculated in the 3D thermo-chemical analysis of the pultrusion. The process induced residual stresses and distortions are predicted in a 2D quasi-static mechanical analysis in which the generalized plane strain elements are utilized in ABAQUS [26]. A 3D transient Eulerian thermo-chemical analysis is coupled with a 2D quasi-static Lagrangian plane strain mechanical analysis of the pultrusion process [24]. The temperature- and cure-dependent resin modulus is calculated using the cure hardening instantaneous linear elastic (CHILE) approach provided in [27].

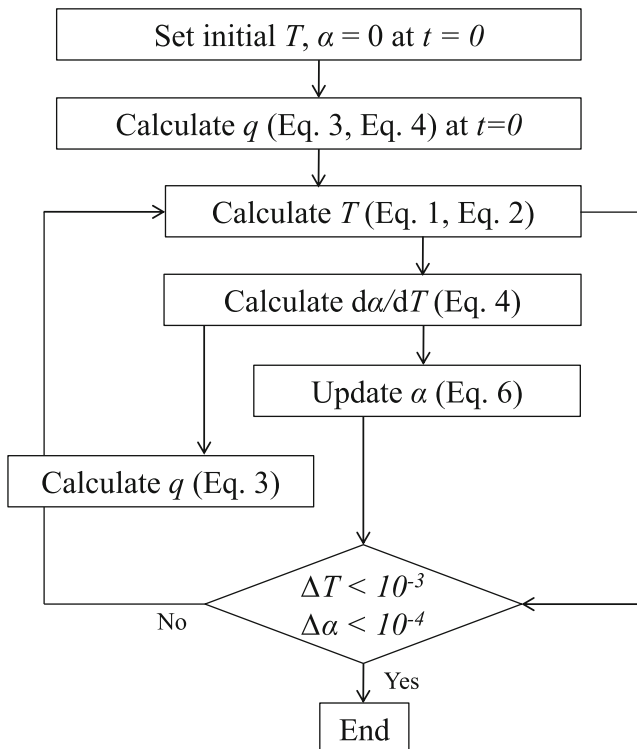


Fig. 2 Flowchart of the iteration procedure to reach the steady state while solving the equation system for the temperature and the degree of cure

Table 1 Thermal properties used in the process simulation [12, 14]

	ρ [kg/m ³]	C_p [J/kg K]	k_{x_1} [W/m K]	k_{x_2}, k_{x_3} [W/m K]
Composite $V_f = 0.639$	2090.7	797.27	0.9053	0.5592
Steel die	7833	460	40	40

Numerical implementation

Energy and cure kinetics equations

The 3D transient energy equations for the composite and the die are given in Eq. 1 and Eq. 2, respectively for the thermo-chemical simulation of the pultrusion process. Here, x_1 is the pulling (longitudinal) direction; x_2 and x_3 are the transverse directions.

$$\rho_c C_p c \left(\frac{\partial T}{\partial t} + u \frac{\partial T}{\partial x_1} \right) = k_{x_1,c} \frac{\partial^2 T}{\partial x_1^2} + k_{x_2,c} \frac{\partial^2 T}{\partial x_2^2} + k_{x_3,c} \frac{\partial^2 T}{\partial x_3^2} + q \tag{1}$$

$$\rho_d C_p d \frac{\partial T}{\partial t} = k_{x_1,d} \frac{\partial^2 T}{\partial x_1^2} + k_{x_2,d} \frac{\partial^2 T}{\partial x_2^2} + k_{x_3,d} \frac{\partial^2 T}{\partial x_3^2} \tag{2}$$

where T is the temperature, t is the time, u is the pulling speed, ρ is the density, C_p is the specific heat, k_{x_1} , k_{x_2} and k_{x_3} are the thermal conductivities in the x_1 -, x_2 - and x_3 -direction, respectively. The subscripts c and d correspond to the composite and the die, respectively. Lumped material properties are used and assumed to be constant. The volumetric internal heat generation (q) [W/m³] due to the exothermic reaction of the epoxy resin can be expressed as [12]:

$$q = (1 - V_f) \rho_r H_{tr} R_r(\alpha, T) \tag{3}$$

where V_f is the fiber volume fraction, ρ_r is the resin density, H_{tr} is the total heat of reaction during the complete cure of the resin sample which is obtained by using a Differential Scanning Calorimetry (DSC) analysis [14]. $R_r(\alpha, T)$ is the rate of degree of cure $d\alpha/dt$ defined by an Arrhenius type of relation and expressed in Eq. 4. Generally, the rate of cure degree is linearly correlated with the heat rate ($dH(t)/dt$) generated during the curing of the resin sample

and the corresponding relation is given in Eq. 4. $dH(t)/dt$ is also obtained from the DSC analysis.

$$R_r(\alpha, T) = \frac{d\alpha}{dt} = \frac{1}{H_{tr}} \frac{dH(t)}{dt} = K_o \exp\left(-\frac{E}{RT}\right) (1 - \alpha)^n \tag{4}$$

where K_o is the pre-exponential constant, E is the activation energy, R is the universal gas constant and n is the order of reaction (kinetic exponent). K_o , E , and n can be obtained by a curve fitting procedure applied to the experimental data evaluated using the DSC [14].

The cure rate in (Eq. 4) can be written as:

$$\frac{d\alpha}{dt} = \frac{\partial \alpha}{\partial t} + \frac{\partial \alpha}{\partial x_1} \frac{dx_1}{dt} = \frac{\partial \alpha}{\partial t} + u \frac{\partial \alpha}{\partial x_1} \tag{5}$$

and from Eq. 5, the resin kinetics equation can be expressed in the Eulerian frame as:

$$\frac{\partial \alpha}{\partial t} = R_r(\alpha, T) - u \frac{\partial \alpha}{\partial x_1} \tag{6}$$

which is used in the thermo-chemical model.

The temperature and the degree of cure distributions at steady state are calculated in ABAQUS. The non-linear internal heat generation (Eq. 3) together with the resin kinetics equation (Eq. 6) is coupled with the energy equation (Eq. 1) in an explicit manner in order to obtain a straightforward and fast numerical procedure. This procedure is performed until the steady state conditions are satisfied. The corresponding procedure is given as a flowchart in Fig. 2. The degree of cure is subsequently updated explicitly for each control volume using Eq. 6 in its discretized form. To reach the steady state conditions, the convergence limits of the temperature and the degree of cure are defined to be 0.001 °C and 0.0001, respectively as seen in Fig. 2. In order to obtain a stable result and to overcome the possible oscillatory behaviour in the numerical implementation, the *upwind scheme* is used for the term ($u\partial\alpha/\partial x_1$) in the resin kinetics equation [20].

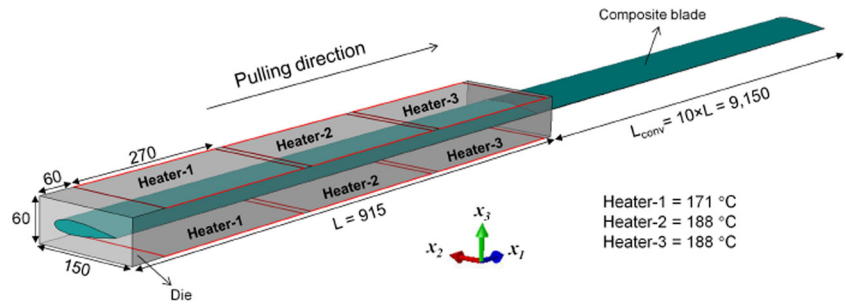
Incremental residual stress implementation

The CHILE model given in Eq. 7 [27] is implemented for the calculation of the instantaneous resin elastic modulus

Table 2 Epoxy resin kinetic parameters [12, 14]

H_{tr} [kJ/kg]	K_o [1/s]	E [kJ/mol]	n
324	192,000	60	1.69

Fig. 3 Schematic view of the pultrusion set-up (Unscaled). All dimensions are in mm



development.

$$E_r = \begin{cases} E_r^0 & T^* \leq T_{C1} \\ E_r^0 + \frac{T^* - T_{C1}}{T_{C2} - T_{C1}}(E_r^\infty - E_r^0) & \text{for } T_{C1} < T^* < T_{C2} \\ E_r^\infty & T_{C2} \leq T^* \end{cases} \quad (7)$$

where E_r^0 and E_r^∞ are the uncured and fully cured resin moduli, respectively. T_{C1} and T_{C2} are the critical temperatures at the onset and completion of the glass transition, respectively, T^* represents the difference between the instantaneous glass transition temperature (T_g) and the resin temperature, i.e. $T^* = T_g - T$ [27]. The evolution of the T_g as a function of degree of cure is modelled by the Di Benedetto equation [28] and expressed as:

$$\frac{T_g - T_{g0}}{T_{g\infty} - T_{g0}} = \frac{\lambda\alpha}{1 - (1 - \lambda)\alpha} \quad (8)$$

where T_{g0} and $T_{g\infty}$ are the glass transition temperatures of uncured and fully cured resin, respectively, λ is a constant used as a fitting parameter.

The effective mechanical properties including the CTEs and the chemical shrinkage strains together with the thermal strains are calculated using the self consistent field micromechanics (SCFM) approach provided by Bogetti and Gillespie [29]. Incremental linear elastic approach is used for the calculation of the residual stresses and distortions as

suggested in [27]. The incremental process induced strain ($\dot{\epsilon}^{pr}$), which is composed of the incremental thermal strain ($\dot{\epsilon}^{th}$) and the chemical shrinkage strain ($\dot{\epsilon}^{ch}$), is defined for the stress-strain relation [24]. The incremental total strain ($\dot{\epsilon}^{tot}$) is defined as the sum of the incremental mechanical strain ($\dot{\epsilon}^{mech}$), $\dot{\epsilon}^{th}$ and $\dot{\epsilon}^{ch}$ and written as:

$$\dot{\epsilon}_{ij}^{tot} = \dot{\epsilon}_{ij}^{mech} + \dot{\epsilon}_{ij}^{th} + \dot{\epsilon}_{ij}^{ch} \quad (9)$$

The incremental stress tensor $\dot{\sigma}_{ij}$ is calculated using the material Jacobian matrix (\mathbf{J}) based on the incremental mechanical strain tensor $\dot{\epsilon}_{ij}^{mech}$ in ABAQUS [26] and the corresponding expression is given as:

$$\dot{\sigma}_{ij} = \mathbf{J}\dot{\epsilon}_{ij}^{mech} \quad (10)$$

The details of the relations between the stress and strain tensors used in the present finite element implementation can be found in [24].

Pultrusion process model

Thermo-chemical analysis

A 3D transient thermo-chemical analysis of the pultrusion process is carried out for a UD NACA0018 blade profile using a Eulerian frame of reference. The pultrusion model is taken from similar set-ups available in the literature [12, 14, 24]. A glass/epoxy based composite and steel are used for the blade and the die block, respectively. The material properties of the composite and the resin kinetic parameters are listed in Table 1 and Table 2, respectively. The fiber volume fraction (V_f) of the composite is 0.639 [14]. A schematic view of the process set-up is shown in Fig. 3. The length of the die and the post die (L_{conv}) are determined to be 0.915 m and 9.15 m, respectively. Cooling channels are located 100 mm under the first heating regions [12, 14]. Hence, all the nodes at the layers D-D and E-E indicated in Fig. 3 are set to the temperature of the cooling water (50 °C) during the whole process. Three heating zones having prescribed set temperatures of 171–188–188 °C [12, 14] are defined as seen in Fig. 3. The spacing between the heating zones is 15 mm. The temperature and the degree

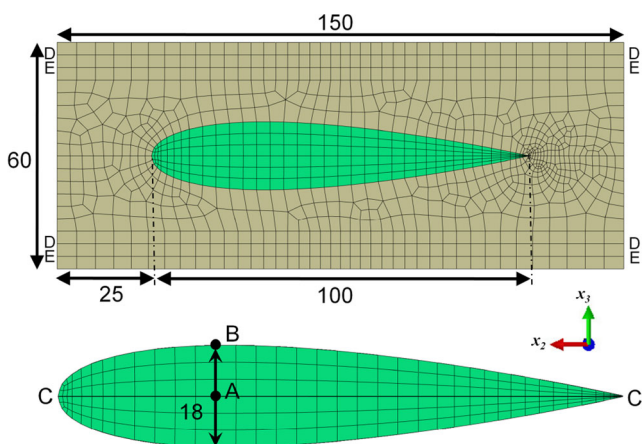
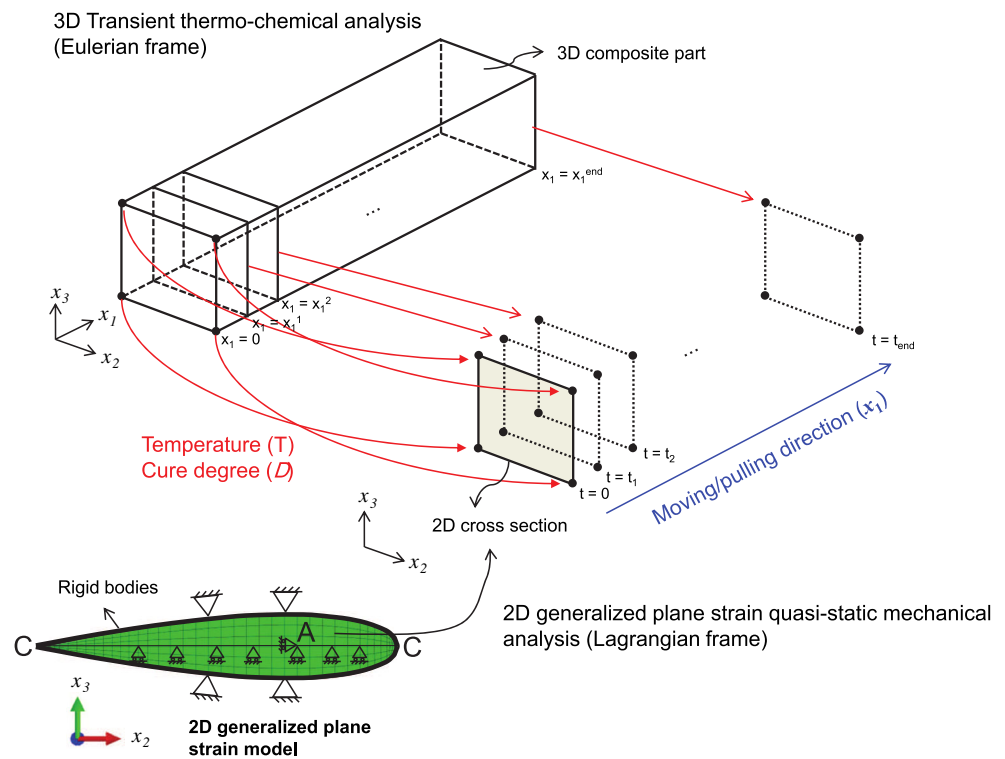


Fig. 4 Cross sectional details of the die (top) and the NACA0018 blade (bottom). All dimensions are in mm

Fig. 5 Representation of the sequential coupling of the 3D thermo-chemical model with the 2D generalized plain-strain mechanical model



of cure of the composite at the die inlet are set to 30 °C (resin bath temperature) and 0, respectively. The remaining exterior surfaces of the die are exposed to ambient temperature with a convective heat transfer coefficient of 10 W/m²-K except for the surfaces located at the heating regions. Similar convective boundaries are also defined for the outer surfaces of the pultruded profile at the post die region. The details of the cross section and the meshing are depicted in Fig. 4 for the part and the die. It is seen that the chord length of the processed NACA0018 blade is 100 mm and the maximum thickness of the cross section is 18 mm. An element length of 15 mm is used in the pulling direction.

Thermo-chemical-mechanical analysis

In the 2D quasi-static mechanical analysis the cross section of the blade is assumed to be moved through the pulling direction (Lagrangian frame) meanwhile tracking the corresponding temperature and degree of cure profiles calculated

in the 3D thermo-chemical analysis (Eulerian frame). A representation of the coupling of the 3D thermo-chemical model with the 2D generalized plane strain mechanical model is shown in Fig. 5 [24]. A plane strain assumption is considered in the analysis since the length of the processing profile (≈ 10 m) is much higher than the cross sectional dimensions (0.1 m). Quadratic generalized plane strain elements are employed in ABAQUS. The constituent mechanical properties are listed in Table 3 and the material properties used in the CHILE approach are given in Table 4.

The rigid body surfaces are defined instead of modelling the whole meshing of the die, since the die is assumed to be rigid as compared to the part. A mechanical contact formulation is employed between the rigid surfaces and the part which allows separation at the interface due to the chemical shrinkage or the thermal contraction. However, any expansion of the part beyond the tool interface is restricted. Note that the friction force at the contact condition is assumed to be zero (sliding condition). A schematic

Table 3 The mechanical properties of the glass fiber and the epoxy resin [29]

	Young's Modulus [GPa]	Poisson's Ratio	CTE [ppm/°C]
Glass fiber	73	0.22	5.04
Epoxy resin (glassy state)	3.447	0.35	57.6

Table 4 The parameters used in the CHILE approach (Eq. 7) and in the calculation of the glass transition temperature (Eq. 8) [24, 27–29]

T_{C1} [°C]	T_{C2} [°C]	E_r^0 [MPa]	E_r^∞ [MPa]	λ	T_{g0} [°C]	$T_{g\infty}$ [°C]
-45.7	-12	3.447	3.447e3	0.4	0	195

view of the generalized plane strain model including the rigid surfaces and the mechanical boundary conditions (BCs) are shown in Fig. 5. A symmetric mechanical BC on the line C-C shown in Fig. 5 is applied in the x_3 -direction. In addition, the point A shown in Fig. 5 is assumed to be also fixed in the x_2 -direction based on the assumption that the innermost region of the composite behaves more stationary as compared with the outermost regions. In the present study the total volumetric shrinkage of the epoxy resin is assumed to be 6% [30].

Results and discussions

The temperature and the degree of cure developments are predicted in the 3D thermo-chemical analysis of the pultrusion and the results are depicted in Fig. 6 for certain points on the pultruded blade, i.e. point A and B. Note that these points are located at the thickest section of the part seen in Fig. 4. The corresponding contour plots are shown in Fig. 7 for the blade cross section at the die exit ($x_1 = 0.915$ m) and at the end of the process ($x_1 \approx 10$ m). The pulling speed is

Fig. 6 The temperature (*top*) and the degree of cure (*bottom*) developments at point A and B

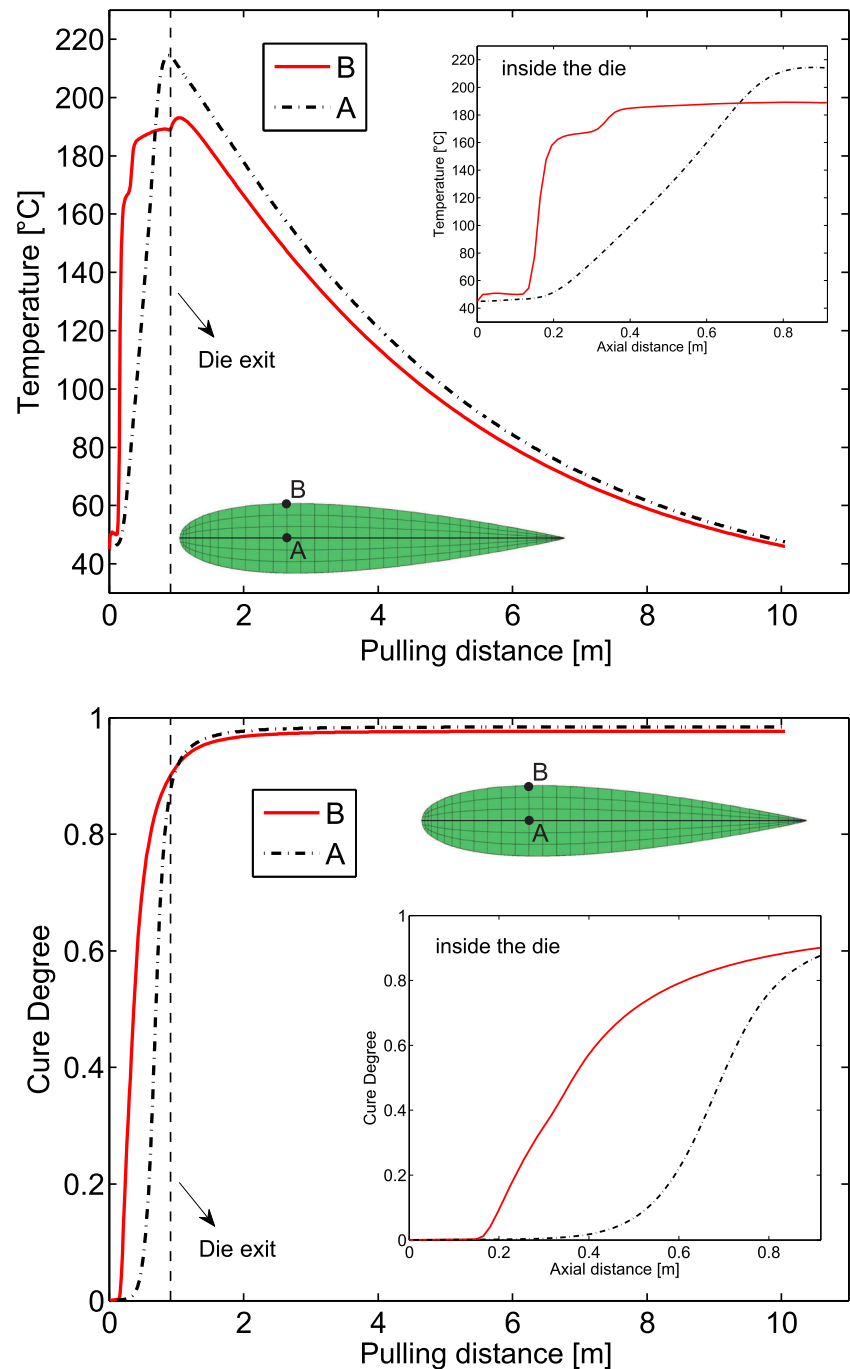
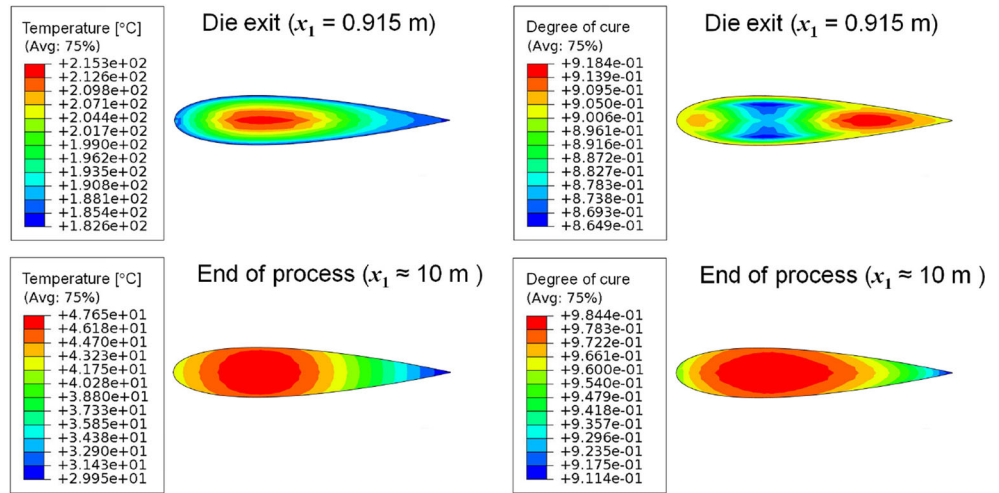


Fig. 7 The contour plots of the temperature (*left*) and the degree of cure (*right*) at the die exit ($x_1 = 0.915$ m) and end of the process ($x_1 \approx 10$ m). Note that the legend of the plots is not same



set to 200 mm/min. It is seen that a non-uniform temperature and degree of cure distributions are found to prevail over the cross section of the part. It is seen from Fig. 6 that point B cures earlier than point A since it is closer to the heaters. The thinner regions of the part have a higher degree of cure value as compared with the thicker regions as seen from the contour plot in Fig. 7 (the degree of cure at the die exit). At the post die region the curing continues increasing since the temperature of the blade is high enough to generate internal

heat after the die exit. Therefore, the entire part is found to be almost fully cured at the end of the process, i.e. the mean degree of cure is found to be approximately 0.97 at the end of the process. The maximum temperature is calculated as around 215 °C near the die exit.

The calculated temperature and the degree of cure fields are mapped to the 2D quasi-static mechanical analysis. The development of the transverse process induced residual stresses are predicted and the results are depicted in Fig. 8

Fig. 8 The development of the process induced stresses for point A and B

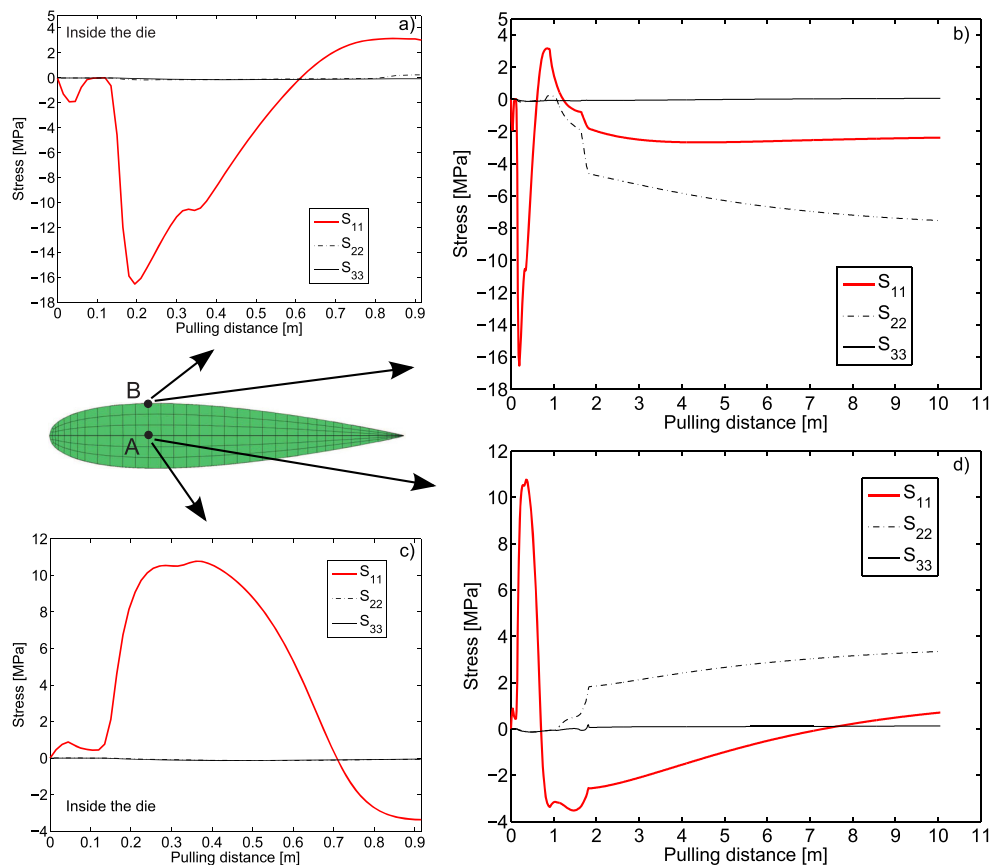
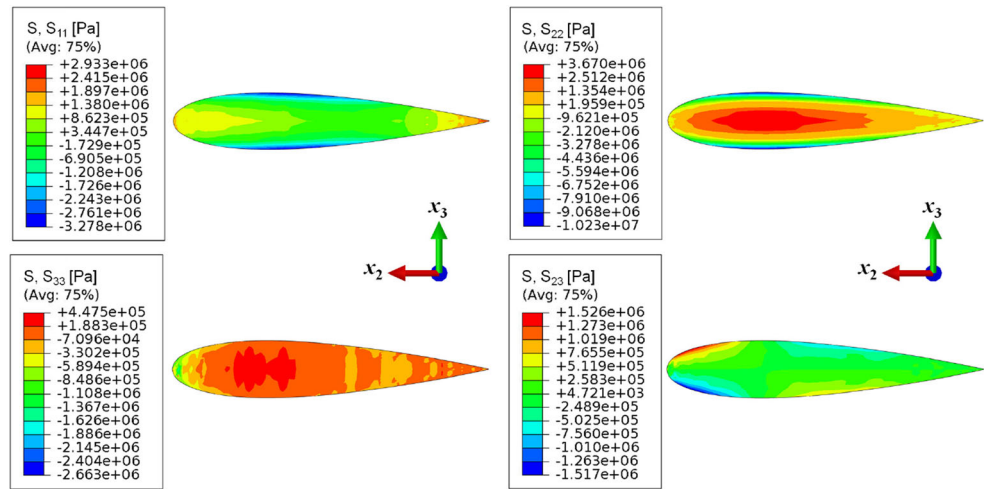


Fig. 9 The undeformed contour plots of the longitudinal normal stress (S_{11}), the transverse normal stresses (S_{22} and S_{33}) and the transverse shear stress (S_{23}) at the end of the pultrusion process. Note that the legend of the plots is not same



for the points A and B. Here, S_{11} is the normal stress in the x_1 -direction (longitudinal), S_{22} and S_{33} are showing the normal stresses in the x_2 -direction (horizontal, transverse) and in the x_3 -direction (vertical, transverse), respectively. Note that the results should be seen together with the temperature and the cure degree curves given in Fig. 6. The overall residual stress evolution at point A and B can be explained as follows: The region closest to the heaters (e.g. point B) cures first which poses a constraint against the inner regions (e.g. point A) of the pultruded profile. Due to this, compression is exhibited towards the regions near the die. When the internal region starts curing rapidly, due to the internal constraint against the outer region, tension and compression prevail at the inner and outer regions, respectively. This can be seen in Fig. 8b,d that point A is under tension and point B is under compression at the end of the process, while upholding the self static equilibrium in which there is no applied external load to the processing part. It is found that the longitudinal

stress values are found to be higher than the transverse stress values inside the die. However, this turns out to be the other way around at the end of the process. Regarding the transverse stresses, the magnitude of the overall S_{33} values are found to be smaller than the S_{22} values since the thickness of the profile (18 mm) is thinner than the chord of the profile (100 mm). The corresponding contour plots of S_{11} , S_{22} and S_{33} together with S_{23} (transverse shear stress on the x_2x_3 plane) are shown in Fig. 9 for the end of the process. The magnitude of S_{23} is found to be smaller than the magnitude of the normal stresses.

The deformation field is given as a deformed contour plot of the composite cross section at the end of the process in Fig. 10. The maximum process induced distortions are calculated approximately as 0.39 mm and 0.066 mm in the x_2 - and x_3 -direction, respectively.

The predicted effective mechanical properties at the end of the process are given in Table 5 for the pultruded NACA0018 blade which is in the glassy state. Here, E is the elastic modulus, G is the shear modulus, ν is the Poisson's ratio and α_i 's are the CTEs. It is seen that the fibers play more significant role for the development of the mechanical properties in the longitudinal direction such as E_1 , ν_{12} and α_1 . On the other hand, E_2 , G_{12}

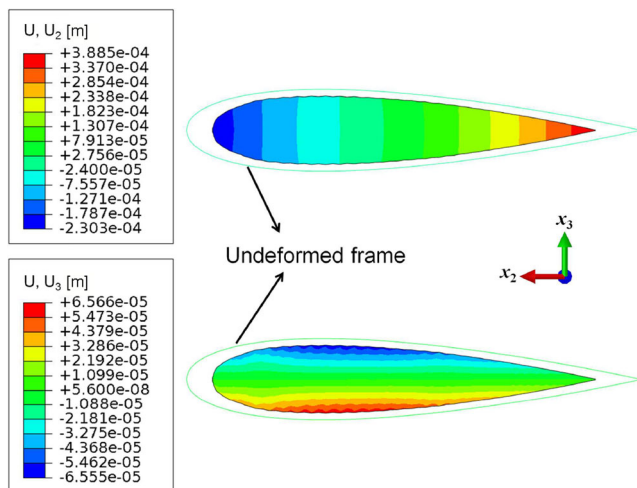
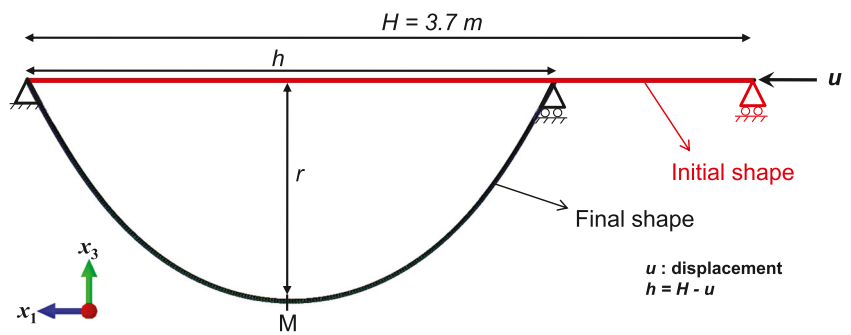


Fig. 10 The deformed contour plots for the residual displacement field obtained at the end of the pultrusion simulation

Table 5 The mechanical properties of the UD composite at fully cured glassy state. ν_f is 0.639 for the predicted values and 0.6 for the measured values [31]

	Predicted (SCFM)	Measured [31]	Unit
E_1	48.2	45.6	GPa
$E_2 = E_3$	12.4	16.2	GPa
$G_{12} = G_{13}$	4.42	5.83	GPa
$\nu_{12} = \nu_{13}$	0.261	0.278	
α_1	6.4	8.6	ppm/°C
$\alpha_2 = \alpha_3$	30.3	26.4	ppm/°C

Fig. 11 A schematic view of the subsequent loading scenario (i.e. bending of the blades)



and α_2 are dominated by the resin matrix as expected. The predicted values are compared with the experimental values taken from literature [31] for a UD glass/epoxy laminate with $V_f = 60\%$. It is seen from Table 5 that a good agreement is found showing that the implementation of the SCFM approach gives reasonable results for the calculation of the effective mechanical properties of the processing composite. The slight difference between the predicted and the measured properties is due to the difference in V_f .

Preliminary structural bent-in place simulations

Model description

In the subsequent loading scenario the transversely isotropic pultruded blade profile is assumed to be bent into Darrieus shape (i.e. arched-blades) taking the residual stresses into account. A schematic view of the bent-in place simulation of the blade is shown in Fig. 11. The bent shape is obtained

by applying a displacement on one end of the profile having an initial total length of 3.7 m and keeping the other end fixed (i.e. hinged BC). In Darrieus type VAWTs, the length/diameter ratio of the rotor, i.e. $h/(2r)$ seen in Fig. 11, has an important effect on the aero dynamical behaviour of the turbines. In the present study, $h/(2r) \approx 2.64$ is used by applying a displacement (u in Fig. 11) value of approximately 0.3 m. The length (h) and the radius (r) of the rotor at the end of the simulation are approximately 3.4 m and 0.645 m, respectively. The obtained $h/(2r)$ is found to be very close to the one used in [4] as 2.7 for a 3-bladed VAWT.

A 3D non-linear structural static analysis is performed by using the quadratic solid elements in ABAQUS. The residual stresses together with the final mechanical properties of the profile predicted in the pultrusion process simulation are transferred to the bending simulation. The residual stresses are treated as a pre-stress condition utilizing the user defined routines in ABAQUS before the bending simulation. This procedure is given in Fig. 12 as a flowchart. Here, it should be noted that the primary equilibrium conditions has to be satisfied in the 3D bending simulation. Therefore, a 3D static equilibrium analysis is carried out without applying

Fig. 12 A flowchart showing the integrated modelling procedure where the manufacturing simulation is coupled with the subsequent loading scenario

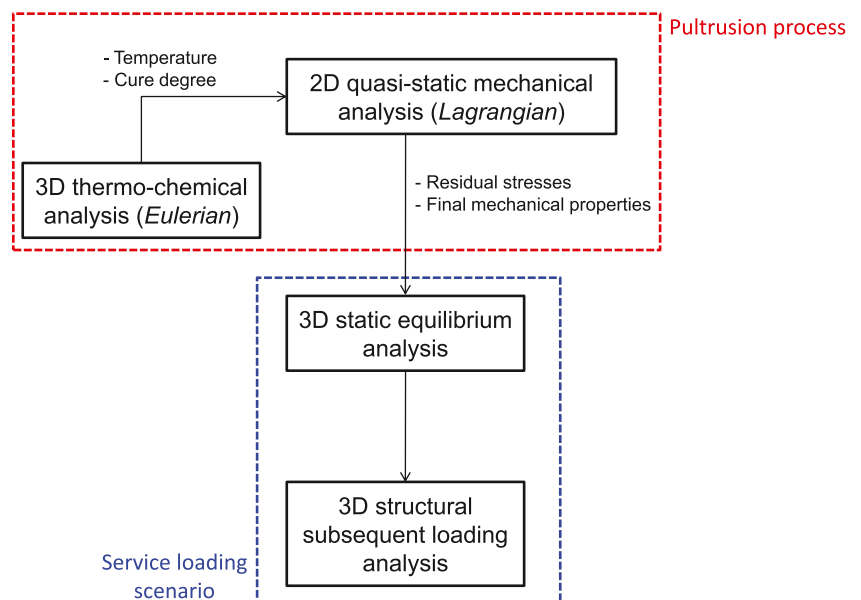


Fig. 13 Contour plots showing the stress distribution with/without residual stresses for section M at the end of the bending simulation. Note that the legend of the plots is not same

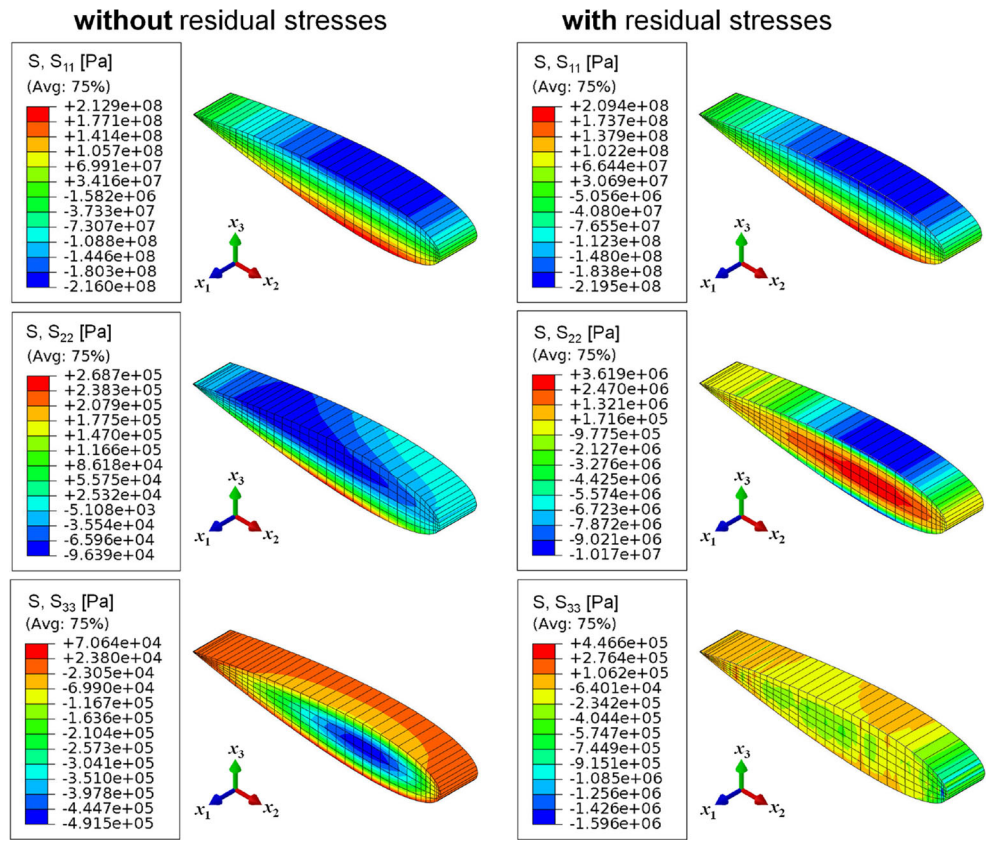
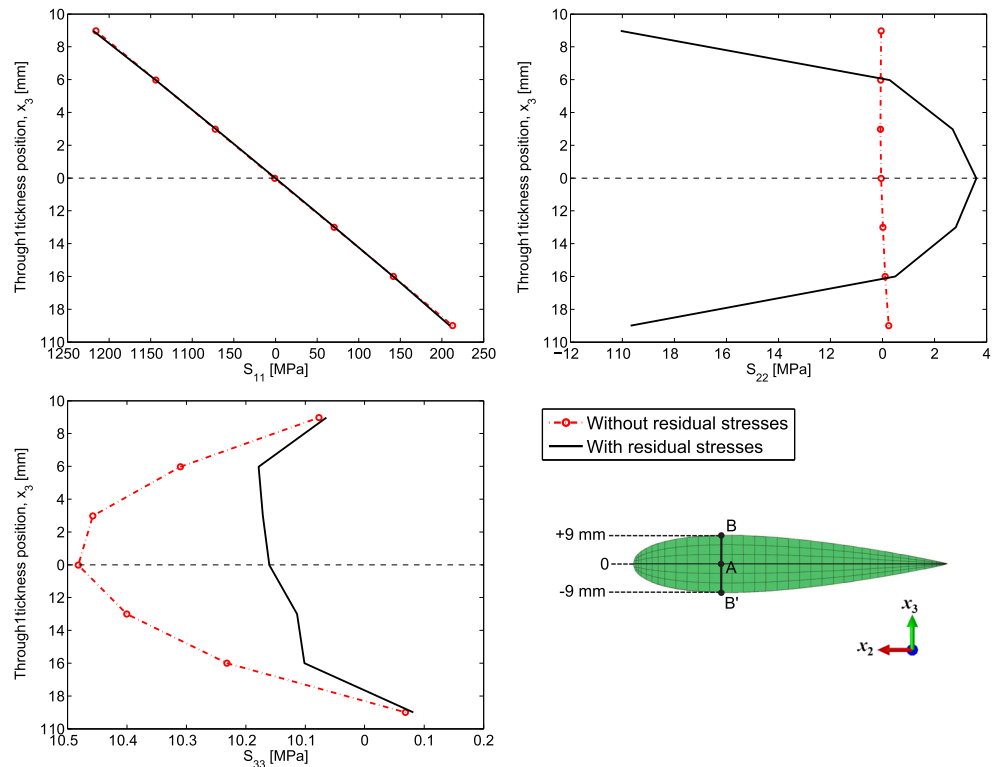


Fig. 14 The through-thickness stress variation at section M with/without residual stresses



any mechanical loads or BCs. The aim is to uphold the stress equilibrium after invoking the pre-stress condition in which the residual stresses are transferred from the process simulation. Subsequently, the loading scenario depicted in Fig. 11 is carried out and the internal stress levels of the bent profile are evaluated.

Results and discussions

The bending simulations are performed taking the residual stresses into account as a pre-stress condition as aforementioned. According to the loading scenario, the maximum normal stresses are expected to be built up at the center of the blade profile (section “M” depicted in Fig. 11) in the longitudinal direction, i.e. x_1 -direction. Hence, the evaluation of the internal stresses at section M are analysed in detail. The contour plots of the normal stresses at section M at the end of the bending simulation are shown in Fig. 13 with and without taking the residual stresses into account. It is seen that the effect of the residual stresses are more dominant for the transverse directions (i.e. for S_{22} and S_{33}) as compared with the longitudinal component (S_{11}) which is obviously more critical for this type of loading scenario. The magnitude of S_{11} is found to be much larger than S_{22} and S_{33} as expected. After obtaining the equilibrium state, it is found that the maximum compression stress for S_{11} is increased approximately from 216 MPa to 220 MPa with the residual stresses. However, the S_{11} value for the maximum tensile stress is decreased from approximately 213 MPa to 210 MPa. The stress levels for S_{22} and S_{33} are relatively small as compared to S_{11} . The through-thickness stress variations are given in Fig. 14 for the thickest region of section M. It is seen that the residual stresses promote the S_{22} level; on the other hand the S_{33} level decreases with taking the residual stresses into account. This shows that the residual stresses have the potential to increase or decrease the internal stress level depending on the service loading scenario.

The longitudinal tensile and compressive strength values of the UD glass/epoxy composite for a $V_f = 0.6$ are given as 1280 MPa and 800 MPa, respectively in [31]. The corresponding transverse tensile and compression strength values are 40 MPa and 145 MPa, respectively [31]. The predicted preliminary internal stress levels shown in Fig. 13 are found to be much smaller than the corresponding strength levels given in [31] based on this specific NACA0018 profile.

Conclusions

A 3D thermo-chemical analysis of the pultrusion for a NACA0018 blade profile was first performed to obtain the temperature and the degree of cure profiles during the process. Afterwards, the process induced residual stresses and distortions were predicted in a 2D quasi-static mechanical

analysis of the pultrusion process for the blade. The integrated modelling of the pultruded NACA0018 blade profile was carried out by combining the manufacturing process simulation with the subsequent loading scenario. The predicted residual stresses together with the final mechanical properties of the transversely isotropic pultruded product were transferred to the loading simulation in which a non-linear bent-in place simulation of the blade was performed. The residual stresses were considered as a pre-stress condition using a user defined routines in ABAQUS and the quadratic elements were used in the bending simulation.

Non-uniform temperature and degree of cure distributions were obtained in the 3D thermo-chemical analysis of the pultrusion process. It was found that the curing continued at the post-die region since the temperature of the composite near the die exit was high enough to generate the internal heat. At the end of the process, tensile and compressive stresses were found to prevail at the inner and outer regions of the pultruded profile. The proposed 3D/2D approach was found to be computationally efficient and fast for the calculation of the residual stresses and distortions together with the temperature and the cure distributions in the pultrusion process. This model has a great potential for the future investigation of the process induced residual stresses and distortions of more complex pultruded profiles.

It was found from the bending simulations that the process induced residual stresses have the potential to promote or demote the internal stress levels. The residual stresses have an important effect on the internal stresses in the transverse directions. On the other hand, this effect is less pronounced for the stress level in the longitudinal direction. It is important to characterize the mechanical aspects of the pultrusion process for the subsequent loading analysis. Therefore, pultrusion process parameters have to be determined accordingly in order not to have excessive process induced residual stresses based on a specific service loading.

Acknowledgments This work is a part of DeepWind project which has been granted by the European Commission (EC) under the FP7 program platform Future Emerging Technology.

References

1. Wisnom MR, Gigliotti M, Ersoy N, Campbell M, Potter KD (2006) Mechanisms generating residual stresses and distortion during manufacture of polymermatrix composite structures. *Compos Part A* 37:522–529
2. Ersoy N, Garstka T, Potter K, Wisnom MR, Porter D, Stringer G (2010) Modelling of the spring-in phenomenon in curved parts made of a thermosetting composite. *Compos Part A* 41:410–418

3. Nielsen MW, Schmidt JW, Hattel JH, Andersen TL, Markussen CM (2013) In situ measurement using FBGs of process-induced strains during curing of thick glass/epoxy laminate plate: experimental results and numerical modelling. *Wind Energy* 16(8):1241–1257
4. Sutherland HJ, Berg DE, Ashwill TD (January 2012) A Retrospective of VAWT Technology. Sandia Report, SAND2012-0304
5. Paulsen US, Vita L, Madsen HA, Hattel JH, Ritchie E, Leban KM et al. (2012) 1st DeepWind 5 MW Baseline design. *Energy Procedia* 24:27–35
6. Paulsen US, Madsen HA, Hattel JH, Baran I, Nielsen PH (2013) Design optimization of a 5 MW floating offshore vertical-axis wind turbine. *Energy Procedia* 35:22–32
7. Gorthala R, Roux JA, Vaughan JG (1994) Resin flow, cure and heat transfer analysis for pultrusion process. *J Compos Mater* 28:486–506
8. Ding Z, Li S, Yang H, Lee LJ, Engelen H, Puckett PM (2000) Numerical and experimental analysis of resin flow and cure in resin injection pultrusion (RIP). *Poly Compos* 21(5):762–778
9. Palikhel DR, Roux JA, Jeswani AL (2013) Die-attached versus die-detached resin injection chamber for pultrusion. *Appl Compos Mater* 20(1):55–72
10. Batch GL, Mocosko CW (1993) Heat transfer, cure in pultrusion: model and experimental verification. *AIChE J* 39:1228–1241
11. Joshi SC, Lam YC (2001) Three-dimensional finite element/nodal-control-volume simulation of the pultrusion process with temperature-dependent material properties including resin shrinkage. *Compos Sci Technol* 61:1539–1547
12. Liu XL, Crouch IG, Lam YC (2000) Simulation of heat transfer and cure in pultrusion with a general-purpose finite element package. *Compos Sci Technol* 60:857–864
13. Suratno BR, Ye L, Mai YW (1998) Simulation of temperature and curing profiles in pultruded composite rods. *Compos Sci Technol* 58:191–197
14. Chachad YR, Roux JA, Vaughan JG, Arafat E (1995) Three-dimensional characterization of pultruded fiberglass-epoxy composite materials. *J Reinf Plast Comp* 14:495–512
15. Carlone P, Palazzo GS, Pasquino R. (2006) Pultrusion manufacturing process development by computational modelling and methods. *Math Comput Model* 44:701–709
16. Li S, Xu L, Ding Z, Lee LJ, Engelen H (2003) Experimental and theoretical analysis of pulling force in pultrusion and resin injection pultrusion (RIP) - Part II: modeling and simulation. *J Compos Mater* 37:195–216
17. Moschiar SM, Reboredo MM, Larrondo H, Vazquez A (1996) Pultrusion of epoxy matrix composites: pulling force model and thermal stress analysis. *Poly Compos* 17(6):850–858
18. Carlone P, Baran I, Hattel JH, Palazzo GS (2013) Computational Approaches for Modeling the Multiphysics in Pultrusion Process. *Advances in Mechanical Engineering*, vol. 2013, Article ID 301875 14 pages. doi:10.1155/2013/301875
19. Baran I, Tutum CC, Hattel JH (2013) The effect of thermal contact resistance on the thermosetting pultrusion process. *Compos Part B: Eng* 45:995–1000
20. Baran I, Tutum CC, Hattel JH (2013) Thermo-chemical modelling strategies for the pultrusion process. *App Compos Mat* 20(6):1247–1263
21. Baran I, Tutum CC, Hattel JH (2013) Reliability estimation of the pultrusion process using the first-order reliability method (FORM). *App Compos Mat* 20:639–653
22. Baran I, Tutum CC, Hattel JH (2013) Optimization of the thermosetting pultrusion process by using hybrid and mixed integer genetic algorithms. *App Compos Mat* 20:449–463
23. Tutum CC, Baran I, Hattel JH (2013) Utilizing multiple objectives for the optimization of the pultrusion process. *Key Eng Mat* 554-557:2165–2174
24. Baran I, Tutum CC, Nielsen MW, Hattel JH, Process induced residual stresses and distortions in pultrusion (2013) *Compos Part B Eng* 51:148–161
25. Baran I, Tutum CC, Hattel JH (2013) The internal stress evaluation of the pultruded blades for a Darrieus wind turbine. *Key Eng Mat* 554-557:2127–2137
26. ABAQUS (2011) 6.11 Reference Guide. Dassault Systems
27. Johnston A (1997) An Integrated Model of the Development of Process-Induced Deformation in Autoclave Processing of Composites Structures, Ph.D. thesis. The University of British Columbia, Vancouver
28. Khoun L, Centea T, Hubert P (2010) Characterization methodology of thermoset resins for the processing of composite materials -case study: CYCOM 890RTM epoxy resin. *J Compos Mater* 44:1397415
29. Bogetti TA, Gillespie JW (1992) Process-induced stress and deformation in thick-section thermoset composite laminates. *J Compos Mater* 26(5):626–660
30. Star TF (2000) Pultrusion for engineers. CRC Press
31. Huang ZM (2001) Simulation of the mechanical properties of fibrous composites by the bridging micromechanics model. *Compos Part A* 32:143172